

Day-ahead electricity prices prediction applying hybrid models of LSTM-based deep learning methods and feature selection algorithms under consideration of market coupling

Wei Li^{a,*}, Denis Mike Becker^a

^aNTNU Business School, Norwegian University of Science and Technology, 7491 Trondheim, Norway

Abstract

The availability of accurate day-ahead electricity price forecasts is pivotal for electricity market participants. In the context of trade liberalisation and market harmonisation in the European markets, accurate price forecasting becomes even more difficult to obtain. The increasing power market integration has complicated the forecasting process, where electricity forecasting requires considering features from both the local market and ever-growing coupling markets. In this paper, we apply state-of-the-art deep learning models, combined with feature selection algorithms for electricity price prediction under the consideration of market coupling. We propose three hybrid architectures of long-short term memory (LSTM) deep neural networks and compare the prediction performance, in terms of various feature selections. In our empirical study, we construct a broad set of features from the Nord Pool market and its six coupling countries for forecasting the Nord Pool system price. The results show that feature selection is essential to achieving accurate prediction. Superior feature selection algorithms filter meaningful information, eliminate irrelevant information, and further improve the forecasting accuracy of LSTM-based deep neural networks. The proposed models obtain considerably accurate results.

Keywords: Deep learning, Electricity price forecasting (EPF), Electricity market coupling, Feature selection, Long short-term memory (LSTM), The Nord Pool system price

1. Introduction

Over the last two decades, worldwide energy markets have experienced a transition towards deregulation and globalisation [1]. Under trade liberalisation, the traditional vertically integrated power utilities are replaced with decentralised business entities whose targets are to maximise their profits. Consequently, a growing number of market participants are exposed to intense competition, and their need for suitable decision support models to increase margins and reduce risk has significantly increased [2]. The availability of accurate day-ahead electricity price forecasts is vital for market participants to adjust production plans and perform effective bidding strategies to make an economic profit. In addition, accurate electricity price forecasting (EPF) can contribute to the stability of the electrical grid with an increase in renewable and remote generation. In particular, volatile prices may overstress power infrastructures to use strategic reserves and create an urgent need to reinforce the grid, resulting in the increased risk of a blackout and voltage collapse.

Due to the productive structure and characteristics of electricity prices, highly accurate forecasting is quite challenging [3, 4]. In this context, price prediction tools are essential for all electricity market participants, to enable them to maximise their profits, mitigate risks, and stabilise the grid under a liberalised and harmonised environment. Numerous research efforts

have contributed to exploiting and developing advanced technologies for day-ahead EPF, aiming at highly accurate forecasting results [5, 6]. A considerable amount of literature has been devoted to EPF methods, which can be classified into five areas [5]: multi-agent [7, 8], fundamental [9, 5], reduced-form [10, 11], statistical [12, 13, 14], and computational intelligence models [15, 16, 17]. In general, computational intelligent (CI) models are state-of-the-art techniques. Compared with other traditional models, their superior performance contributes to the prevalence of CI-based models in EPF.

In recent years, deep neural networks (DNNs) have gradually entered the scientific research related to electricity price forecasting. They are regarded as the most avant-garde CI approach in various other disciplines [18, 19, 20]. DNNs are often categorised into three main classes: Feed-forward Neural Networks (FNNs), Recurrent Neural Networks (RNNs), and Convolutional Neural Networks (CNNs). For time series and sequence prediction, RNNs achieved superior performance by building extra mappings to hold relevant information from past inputs. The long-short term memory (LSTM) and gated recurrent units (GRU) are important variants of this kind of network which overcome the vanishing gradient problem [21]. Due to their superiority in forecasting, researchers gradually pay attention to their application in EPF [22, 23, 24]. However, with the increasing integration of electricity markets, making accurate forecasts becomes even more difficult in the complex and integrated system. A large number of explanatory variables from an ever-growing number of interconnected, neighbouring

*Corresponding author

Email address: wei.n.li@ntnu.no (Wei Li)

power systems need to be considered when forecasting electricity prices. When DNNs are applied on high-dimensional data, a critical issue is known as the curse of dimensionality [25]. It means, with a large number of features, the performance of DNNs will degrade because of overfitting [26]. To the best of our knowledge, no existing study considers how to apply DNNs with huge amounts of high-dimensional data in the ever-growing integrated market. In particular, the curse of dimensionality of the application of the state-of-the-art LSTM deep learning models in EPF, considering market coupling, have yet to be solved. To fill this scientific gap, we propose three hybrid architectures of LSTM-based deep learning predictive models combined with advanced feature selection algorithms: the two-step hybrid architecture, the autoencoder hybrid architecture and the two-stage hybrid architecture. We employ five feature selection algorithms for selecting features from Nord Pool and its neighbouring, interconnected countries. They are: Pearson's correlation (PC), particle swarm optimisation combined with the extreme learning machine method (PSO-ELM), genetic algorithm combined with the extreme learning machine method (GA-ELM), recursive feature elimination together with the support vector regression method (RFE-SVR) and the lasso regression method.

1.1. Contributions

While some current research attempts to involve explanatory variables from integrated markets to make a prediction for electricity price [27, 28, 29], no existing research investigated the state-of-the-art LSTM-based neural networks, which achieved superior performance for time series forecasting. Besides, some research starts to pay attention to the market integration in Nord Pool [30, 31, 32]. However, efficient ways to utilise the ever-growing information from its integrated markets for EPF have yet to be explored. We therefore propose a collection of LSTM-based models with various feature selection algorithms and compare their forecasting performance. The main contributions are as follows:

1. We introduce three architectures of hybrid LSTM-based deep neural networks for EPF, and conclude that different feature selections algorithms collect a divergent subset of features, which in turn affects the proposed LSTM models' prediction accuracy.
2. The EPF of the Nord Pool market under consideration of market coupling with the application of deep learning methods remains unexplored. We compare and analyse the forecasting performance of the proposed models in the case study of the Nord Pool system price forecasting, considering six integrated markets (sixty-two features).
3. We employ a SHAP game theoretic approach to explore the relevance of various cross-border features in EPF.

The remainder of this paper is organised as follows. Section 2 describes the dataset used in this research. In Section 3, we present the architectures of hybrid models. In Section 4, we describe the proposed theoretical concepts of feature selection



Figure 1 A map of the overview of the Nord Pool market coupling.

methods. The autoencoder LSTM models are described in Section 5. Section 6 describes the model training and introduces evaluation criteria applied in our analysis. Section 7 reports the forecasting results of the implemented models for the Nord Pool market day-ahead price. Finally, Section 8 concludes the paper and proposed future research developments.

2. Data description

This paper discusses and evaluates several hybrid LSTM-based approaches for the prediction of the Nordic hourly and daily system prices. Each hourly system price is calculated as a market-clearing price without taking into account any congestion restrictions. The daily system price represents the arithmetic average of the 24 hourly prices. It is used as a settlement price for the derivatives market.

Previous empirical research on the prediction of electricity prices has considered both market-related information and supply/demand relations. The former type includes spot prices and exchange rates. The latter concerns production, consumption, and their prognosis. To find out what matters when predicting the day-ahead Nordic system price in coupling markets, we also include the electricity exchange between Nord Pool and its integrated countries. The Russian electricity market is excluded because it differs significantly from European models. To consider the influence of the correspondence between electricity flow and capacity, we introduce a new daily feature, namely the cross-border flow deviation. It can be calculated as $\sigma = \sqrt{\sum_{i=1}^N (X_i - \mu_i)^2 / N}$, where X_i is the hourly electricity flow, μ_i is the hourly expected exchange capacity, and N stands for 24 hours.

2.1. Data set

We collected data from the Nord Pool¹, Thomson Reuters Eikon² and Entsoe³. The available time series ranges from

¹Nord Pool: <https://www.nordpoolgroup.com/>

²Thomson Reuters Eikon: <https://eikon.thomsonreuters.com/>

³Entsoe: <https://transparency.entsoe.eu/>

01/01/2015 to 31/12/2019. We consider eight categories of input features: day-ahead price, production, production prognosis, consumption, consumption prognosis, currency exchange rate, cross-border electricity flow, and flow deviation. Nord Pool also provides cross-border transmissions with Germany (DE), the Netherlands (NL), Lithuania (LT), Estonia (EE), Poland (PL), and Russia (RU). The map in Figure 1 shows both the Nord Pool markets as well as transmissions (black dashed lines) between the Nord Pool and its coupling bidding areas. Five bidding zones in Norway (NO1, NO2, NO3, NO4, and NO5), Sweden (SE1, SE2, SE3, and SE4), and two in Denmark (DK1 and DK2) and one in Finland. Since the transmissions between DK1 and NL started at 01/09/2019, the data series is not sufficient for the application of DL models. Besides, the electricity exchange between SE4 and LT started at 09/12/2015. Therefore, the entire available dataset employed in this study ranges from 09/12/2015 to 31/12/2019. The features included in the dataset are shown in Table 1. The hourly data is converted into the daily data by the arithmetic average (e.g. price) or the aggregate (e.g. flow).

2.2. Cross-border electricity transmission

Figure 2 shows the electricity exports from Germany, the Netherlands, Lithuania, Poland, and Russia in 2019⁴. The exports to the Nord Pool comprised 16.03% of the whole exports from these coupling countries. In Figure 3, we can see that the electricity exports of the Nord Pool comprised 4.82% of its total production in 2019. The EU aims at achieving 15% interconnection capacity in 2030 for each EU country [33].

Table 1 The features included in the dataset.

Feature	Description (Units)	Data Source
F1	System Day-ahead price 1-Lag (EUR/MWh)	Nord Pool
F2	SE1 Day-ahead price (EUR/MWh)	Nord Pool
F3	SE2 Day-ahead price (EUR/MWh)	Nord Pool
F4	SE3 Day-ahead price (EUR/MWh)	Nord Pool
F5	SE4 Day-ahead price (EUR/MWh)	Nord Pool
F6	FI Day-ahead price (EUR/MWh)	Nord Pool
F7	DK1 Day-ahead price (EUR/MWh)	Nord Pool
F8	DK2 Day-ahead price (EUR/MWh)	Nord Pool
F9	NO1 Day-ahead price (EUR/MWh)	Nord Pool
F10	NO2 Day-ahead price (EUR/MWh)	Nord Pool
F11	NO3 Day-ahead price (EUR/MWh)	Nord Pool
F12	NO4 Day-ahead price (EUR/MWh)	Nord Pool
F13	NO5 Day-ahead price (EUR/MWh)	Nord Pool
F14	EE Day-ahead price (EUR/MWh)	Nord Pool
F15	LT Day-ahead price (EUR/MWh)	Nord Pool
F16	PL Day-ahead price (PLN/MWh)	Thomson Reuters Eikon
F17	DE Day-ahead price (EUR/MWh)	Thomson Reuters Eikon
F18	NL Day-ahead price (EUR/MWh)	Thomson Reuters Eikon
F19	Nordic production (MWh)	Nord Pool
F20	EE production (MWh)	Nord Pool
F21	LT production (MWh)	Nord Pool
F22	PL production (MWh)	Entsoe

Continued on next column

Continued from previous column

Feature	Description (Units)	Data Source
F23	DE production (MWh)	Entsoe
F24	NL production (MWh)	Entsoe
F25	Nordic production prognosis (MWh)	Nord Pool
F26	EE production prognosis (MWh)	Nord Pool
F27	LT production prognosis (MWh)	Nord Pool
F28	PL production prognosis (MWh)	Entsoe
F29	DE production prognosis (MWh)	Entsoe
F30	NL production prognosis (MWh)	Entsoe
F31	Nordic consumption (MWh)	Nord Pool
F32	EE consumption (MWh)	Nord Pool
F33	LT consumption (MWh)	Nord Pool
F34	PL consumption (MWh)	Entsoe
F35	DE consumption (MWh)	Entsoe
F36	NL consumption (MWh)	Entsoe
F37	Nordic production prognosis (MWh)	Nord Pool
F38	EE consumption prognosis (MWh)	Nord Pool
F39	LT consumption prognosis (MWh)	Nord Pool
F40	PL consumption prognosis (MWh)	Entsoe
F41	DE consumption prognosis (MWh)	Entsoe
F42	NL consumption prognosis (MWh)	Entsoe
F43	EUR/NOK	Nord Pool
F44	EUR/SEK	Nord Pool
F45	EUR/DKK	Nord Pool
F46	EUR/PLN	Thomson Reuters Eikon
F47	NO2 ↔ NL flow (MWh)	Nord Pool
F48	DK1 ↔ DE flow (MWh)	Nord Pool
F49	DK2 ↔ DE flow (MWh)	Nord Pool
F50	SE4 ↔ DE flow (MWh)	Nord Pool
F51	SE4 ↔ PL flow (MWh)	Nord Pool
F52	SE4 ↔ LT flow (MWh)	Nord Pool
F53	FI ↔ EE flow (MWh)	Nord Pool
F54	FI ↔ Russia flow (MWh)	Nord Pool
F55	NO2 ↔ NL flow deviation	Calculation
F56	DK1 ↔ DE flow deviation	Calculation
F57	DK2 ↔ DE flow deviation	Calculation
F58	SE4 ↔ DE flow deviation	Calculation
F59	SE4 ↔ PL flow deviation	Calculation
F60	SE4 ↔ LT flow deviation	Calculation
F61	FI ↔ EE flow deviation	Calculation
F62	FI ↔ Russia flow deviation	Calculation

3. Architecture of a hybrid model

The architecture of a typical hybrid model for EPF, shown in Figure 4, consists of two steps. The first step includes data processing and feature selection, and the second step consists of training the predictive models and making predictions. When working with recurrent neural networks, there is another type of hybrid model that will turn the input data into a compressed representation rather than specifically show which features are selected. It is called autoencoder architecture, shown in Figure 5. A third network architecture combines the two aforementioned architectures, and it is referred to as two-stage feature selection. Here the explanatory variables will be selected by some feature selection method in the first stage. The selected

⁴Fraunhofer ISE provides the electricity exchange data of Germany/Europe: <https://www.energy-charts.de/>

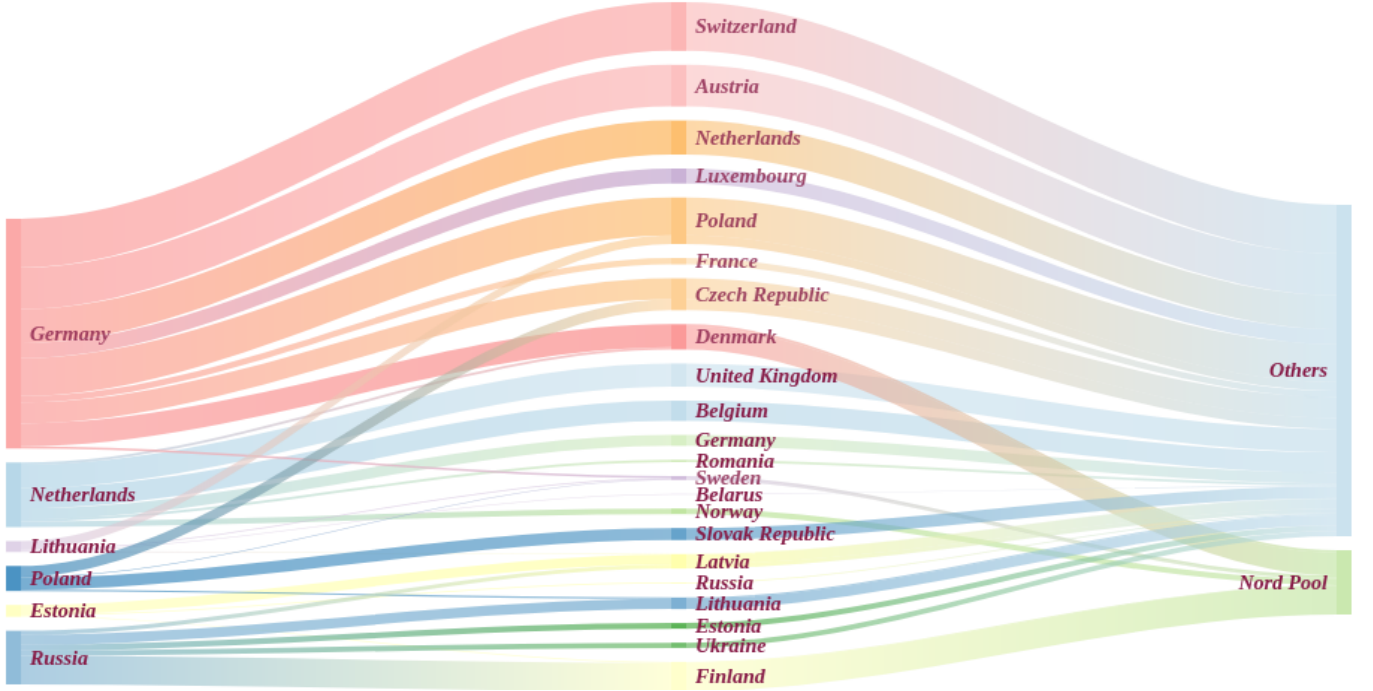


Figure 2 The electricity cross-border transmission from the coupling countries to Nord Pool.

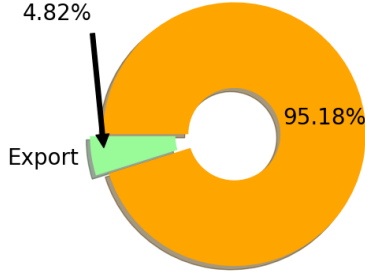


Figure 3 The percentage of the Nord Pool production for exporting.

features will then become the input for the autoencoder models in the second stage. Figure 6 shows this architecture.

3.1. LSTM

The LSTM architecture was initially introduced by [34] and has since been enhanced by other researchers to achieve better performance [35, 36, 37]. An LSTM network is a special kind of a recurrent neural network that is capable of learning long-term dependencies. Unlike simple RNNs, an LSTM network has built-in mechanisms that control how information is memorised or abandoned throughout time. The architecture of the LSTM network is shown in Figure 7 and is defined by the following system of equations [38]:

$$f_t = \sigma_g(W_{xf}x_t + W_{hf}h_{t-1} + W_{cf}c_{t-1} + b_f) \quad (1)$$

$$i_t = \sigma_g(W_{xi}x_t + W_{hi}h_{t-1} + W_{ci}c_{t-1} + b_i) \quad (2)$$

$$o_t = \sigma_g(W_{xo}x_t + W_{ho}h_{t-1} + W_{co}c_{t-1} + b_o) \quad (3)$$

$$c_t = f_t \otimes c_{t-1} + i_t \otimes \sigma_h(W_{xc}x_t + W_{hc}h_{t-1} + b_c) \quad (4)$$

$$h_t = o_t \otimes \sigma_h(c_t) \quad (5)$$

where f_t , i_t , o_t , c_t and h_t indicate the values of the forget gate state, input gate state, output gate state, memory cell and hidden state at time t in the sequence, respectively. σ_g and σ_h are sigmoid function and hyperbolic tangent function and \otimes denotes the element-wise product. Like all RNNs, the LSTM neural networks will process data sequentially. Hence, they take the form of a chain structure, as shown in Figure 8.

4. Feature selection

Feature selection is the process of selecting a subset of relevant features when developing a predictive model. It can reduce the computation time, improves model prediction performance, and helps to get a better understanding of the dataset [39]. The current research on feature selection algorithms can be categorised as filter, wrapper and embedded methods. In this paper, we will explore the following feature selection algorithms: PC (filter method), PSO-ELM (wrapper method), GA-ELM (wrapper method), RFE-SVR (wrapper method) and LASSO regression (embedded method). In addition, we will introduce three autoencoder LSTM methods: LSTM-LSTM Encoder-Decoder, CNN-LSTM Encoder-Decoder and Convolutional-LSTM (ConvLSTM) model.

4.1. PC

PC coefficient is a statistic used to measure the linear relationship between two data samples. Given two variables (X, Y), the formula of the PC coefficient ρ is given by the following:

$$\rho(X, Y) = \frac{\text{cov}(X, Y)}{\sigma_X \sigma_Y} \quad (6)$$

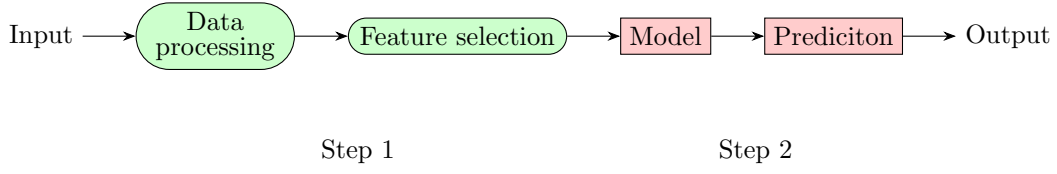


Figure 4 The flowchart of a two-step hybrid model. The green nodes stand for the first step and the red nodes for the second step.

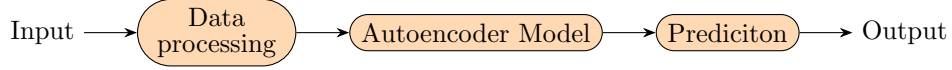


Figure 5 The flowchart of an autoencoder hybrid model. The orange nodes stand for the autoencoder process.

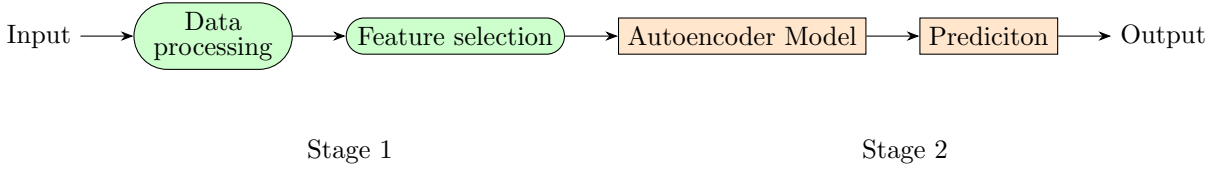


Figure 6 The flowchart of a two-stage hybrid model. The green nodes stand for the first stage and the orange nodes for the second stage.

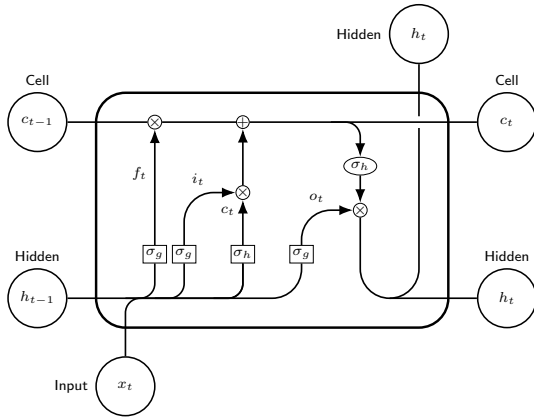


Figure 7 LSTM cell.

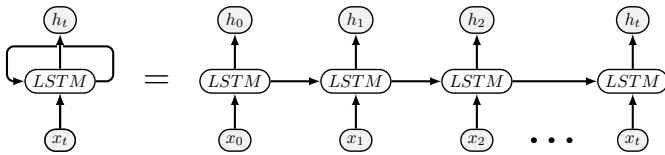


Figure 8 LSTM chain.

where cov is the covariance, σX is the standard deviation of X , and σY is the standard deviation of Y .

4.2. PSO-ELM and GA-ELM

The PSO-ELM and GA-ELM are wrapper-based hybrid methods. PSO and GA are different types of optimisation algorithms which provide the optimised subsets of features as the input to the ELM to detect the optimal feature selection. The

two wrapper-based methods have been widely used for various feature selection problems [40, 41, 42, 43, 44, 45].

ELM is a single hidden layer feedforward neural network. Its fast training [46] contributes to the popularity of its employment as a predictive model in the wrapper-based feature selection [47, 48, 49]. The output of ELM is calculated as follows:

$$f_L(x) = \sum_{i=1}^L \beta_i g(w_i x_j + b_i), j = 1, \dots, N \quad (7)$$

where L is the number of hidden units, N is the number of training samples, β is the weight vector between the hidden layer and the output, w is the weight vector between the input and the hidden layer, $g(*)$ denotes an activation function, b is a bias vector and x is the input vector.

The basic idea of PSO is that a population of particles moves through the search space. Each particle has knowledge about its current velocity, its own past best configuration ($\vec{p}(t)$), and the current global best solution ($\vec{g}(t)$). Based on this information, each particle's velocity is updated such that it moves closer to the global best and its past best solution at the same time. The velocity update is performed according to the following equation:

$$\begin{aligned} \vec{v}(t+1) = & \omega \vec{v}(t) + c_1 r_1 (\vec{p}(t) - \vec{x}(t)) \\ & + c_2 r_2 (\vec{g}(t) - \vec{x}(t)) \end{aligned} \quad (8)$$

where c_1 and c_2 are constants defined beforehand, that determine the significance of $\vec{p}(t)$ and $\vec{g}(t)$. $\vec{v}(t)$ is the velocity of the particle, $\vec{x}(t)$ is the current particle position, r_1 and r_2 are random numbers from the interval $[0,1]$, and ω is a constant ($0 \leq \omega \leq 1$). The new position is calculated by summing the previous position and the new velocity as follows:

$$\vec{x}(t+1) = \vec{x}(t) + \vec{v}(t+1) \quad (9)$$

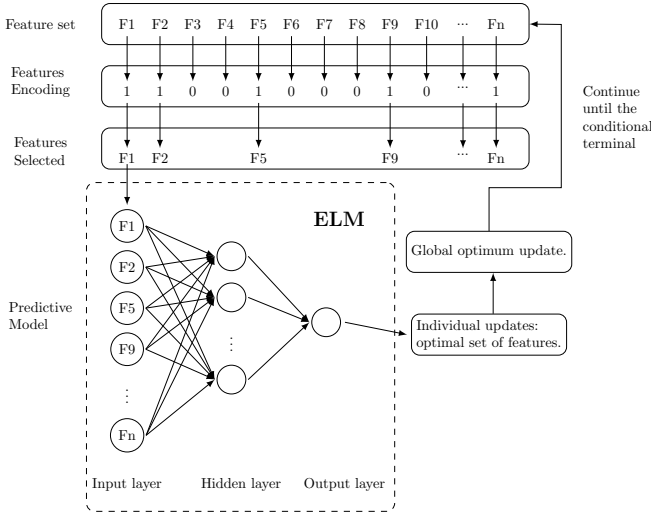


Figure 9 The workflow of two-step-wrapper-based feature selection model.

This iterative process is repeated until a stopping criterion is satisfied.

The genetic algorithm is a search metaheuristic that was inspired by Darwin's theory of natural selection. In general, GAs will search for the optimal solution from a set of possible solutions, called a population. A solution is referred to as a chromosome or an individual. These chromosomes evolve over a number of generations by recombination (cross-over) and mutation [50].

Figure 9 shows the workflow of PSO-ELM and GA-ELM models for feature selection. The process flow of GA-ELM can be described as follows:

- Step 1:** Initialise the population with a set of random individuals, each individual representing a particular subset of features. For a specific individual (feature set), the features are encoded as "1" or "0", as shown in Figure 9. "1" means that the feature is selected and "0" means that it is not selected.
- Step 2:** The selected features are the input for the ELM. The prediction results of the ELM are used to evaluate the fitness value of the individuals. The fitness value is calculated based on the MSE.
- Step 3:** Select the best individual with regard to the fitness value. If its fitness is higher than the lowest value in the existing mating pool, it will replace the individual with the worst fitness. Furthermore, the global optimum will be updated accordingly.
- Step 4:** The child individuals are generated by crossover and mutation. The new generation is composed of a set of new individuals that are encoded and prepared to be evaluated. The whole process continues until meeting the iteration terminal. The best feature subset in the mating pool is the optimal selection.

4.3. RFE-SVR

RFE-SVR is another wrapper-based feature selection method. The core idea of this algorithm is to search for the best subset of features by starting with all features and discarding the less important features.

To minimise the forecasting errors, SVR individualises the hyperplane by maximising the margin. To solve a nonlinear regression problem, the following linear estimation function is considered [51]:

$$f(x) = (w \times \Phi(x)) + b \quad (10)$$

where w is the parameter vector, $\Phi(x)$ is a kernel function and b is a constant. The function formulation of the SVR model can be transformed into the following convex minimisation problem to minimise:

$$\min \frac{1}{2} \|w\|^2 + C \sum_{i=1}^n (\xi_i + \xi_i^*) \quad (11)$$

subject to the constraints:

$$\begin{aligned} (w \times \Phi(x_i) + b) - y_i &\leq \epsilon + \xi_i \\ y_i - (w \times \Phi(x_i) + b) &\leq \epsilon + \xi_i^* \\ \xi_i, \xi_i^* &\geq 0; i = 1, 2, \dots, n \end{aligned}$$

where C is a regularisation constant. ξ_i and ξ_i^* are slack variables, which are used to handle the situation where no such function $f(x)$ exists to satisfy the constraint $|y_i - (w \times x_i + b)| \leq \epsilon$ for all points. They are regarded as the soft margin to allow regression errors ϵ to exist up to ξ_i and ξ_i^* and still satisfy the constraint. Only the points outside the ϵ -radius contribute to the final cost. The error parameter ϵ represents the region of the tube located around the regression function $f(x)$, as shown in Figure 10.

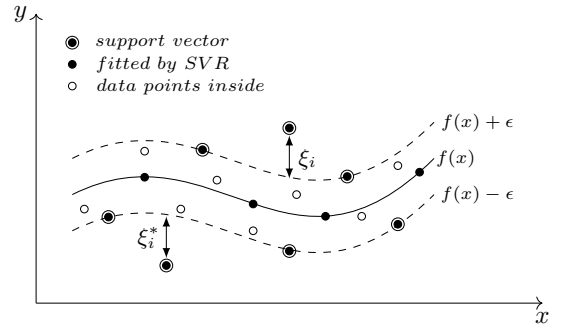


Figure 10 Fitted SVR.

4.4. LASSO regression

The Lasso regression aims at increasing the prediction accuracy of regression models by adding a penalty $\lambda \sum_{i=1}^n |w_i|$ to the loss function. This means that, instead of minimising a loss function $\sum_{j=1}^m (y_j - \sum_{i=1}^n x_{ji} \beta_i)^2$, the loss function to minimise becomes $\sum_{j=1}^m (y_j - \sum_{i=1}^n x_{ji} \beta_i)^2 + \lambda \sum_{i=1}^n |w_i|$, where w is the vector of model coefficients. The algorithm has the advantage that it shrinks some of the less critical coefficients of features to zero. Therefore, it removes less relevant features.

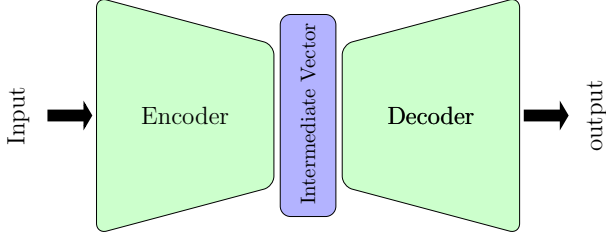


Figure 11 A structure of Encoder-Decoder model.

5. Autoencoder LSTM

An autoencoder is typically a neural network that aims at filtering and compressing the representation of its input, which consists of two components: an encoder and a decoder, shown in Figure 11. The encoder typically accepts a set of the input data and compresses the information into an intermediate vector. The decoder is typically a predictive model. In our case, an LSTM network is a decoder and the encoders are LSTM, CNN, and convolutional layers.

5.1. LSTM-LSTM Encoder-Decoder model

In an LSTM-LSTM Encoder-Decoder model, an LSTM model is used in the encoder to process the raw input time series and transform it to be an intermediate vector. The difference with two-stage methods is that the encoder compresses all of the information into a vector rather than create a vector with selected features. The decoder is an LSTM model and is the same as a predictive model in two-stage methods.

5.2. CNN-LSTM Encoder-Decoder model

In a CNN-LSTM Encoder-Decoder model, a convolutional neural network (CNN) is the encoder to filter the input data. CNNs were originally, and successfully, used to process the image input data in image recognition tasks [52] or the sequence of input data in natural language processing problems [53]. The convolutional layers are usually followed by a pooling layer, which extracts certain values from the convolved features and produces a lower dimensional output value. Then, the output values are flattened into one long intermediate vector. For instance, when passing the input image data through a convolutional layer, the input becomes an abstracted feature map by applying and sliding a convolution kernel (filter) all over the input matrix (a two-dimensional structure with width and height). Unlike images, a convolution layer can be seen applying and sliding a filter over the time series (a one-dimensional structure).

5.3. Convolutional LSTM Encoder-Decoder model

The computational mechanism of the convolutional LSTM (ConvLSTM) is similar to that of CNN-LSTM [54]. Unlike the CNN-LSTM, where the CNN model generates the input for the LSTM model, in the ConvLSTM model, the LSTM neural network processes the extracted information directly from preceding convolutional layers.

6. Experiment details

In this section, we introduce the concepts and methods employed in the process of training and evaluation of the constructed models.

6.1. Evaluation metrics

In this paper, we employ several indicators to evaluate the accuracy of predictions: the mean absolute error (MAE), the root mean squared error (RMSE), the mean absolute percentage error (MAPE) and the symmetric mean absolute percentage error (SMAPE) as the model estimator. They are commonly adopted in EPF research [1]. Given a predicted output vector $\hat{y}_k = [\hat{y}_1, \dots, \hat{y}_N]$ and a real output vector $y_k = [y_1, \dots, y_N]$, the MAE, RMSE, MAPE and SMAPE can be calculated as follows:

$$\text{MAE} = \frac{1}{N} \sum_{k=1}^N |y_k - \hat{y}_k| \quad (12)$$

$$\text{RMSE} = \sqrt{\frac{1}{N} \sum_{k=1}^N (y_k - \hat{y}_k)^2} \quad (13)$$

$$\text{MAPE} = \frac{100}{N} \sum_{k=1}^N \left| \frac{y_k - \hat{y}_k}{y_k} \right| \quad (14)$$

$$\text{SMAPE} = \frac{100}{N} \sum_{k=1}^N \frac{|y_k - \hat{y}_k|}{(|y_k| + |\hat{y}_k|)/2} \quad (15)$$

6.2. Diebold-Mariano test

The metrics for assessing the forecasting accuracy mentioned above cannot guarantee that the observed difference from two predictive models is statistically significant. In this context, the Diebold-Mariano (DM) test is typically used for evaluating the performance of two models [55, 56]. Given the actual values of a time series $[y_t; t = 1, \dots, T]$, two forecasts from two models $[\hat{y}_{1t}; t = 1, \dots, T]$ and $[\hat{y}_{2t}; t = 1, \dots, T]$, and the associated forecast errors $e_{1t} = \hat{y}_{1t} - y_t$ and $e_{2t} = \hat{y}_{2t} - y_t$, the DM test defines the loss differential between the two forecasts by:

$$d_t^{F1, F2} = g(e_{1t}) - g(e_{2t}) \quad (16)$$

where $g(*)$ stands for loss function. In a one-sided DM test, the hypotheses is:

$$\begin{aligned} H_0 : \mathbb{E}(d_t^{F1, F2}) &\geq 0, \\ H_1 : \mathbb{E}(d_t^{F1, F2}) &< 0. \end{aligned} \quad (17)$$

A one-sided DM test is used to detect whether F2 is better than F1. If H_0 is rejected, the test suggests that the accuracy of F1 is, statistically, significantly better than F2. The complementary one-sided DM test can be expressed as follows:

$$\begin{aligned} H_0 : \mathbb{E}(d_t^{F1, F2}) &\leq 0, \\ H_1 : \mathbb{E}(d_t^{F1, F2}) &> 0. \end{aligned} \quad (18)$$

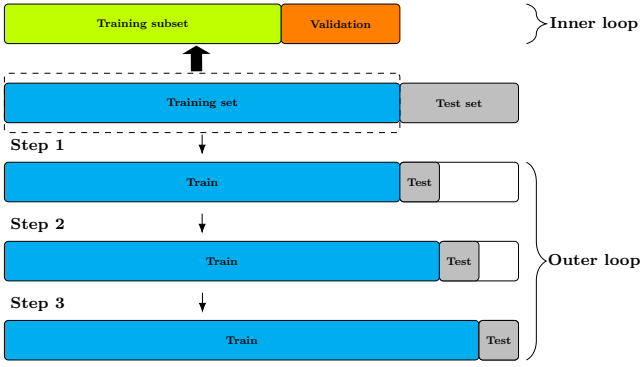


Figure 12 Walk forward nested cross-validation.

If H_0 is rejected, the test suggests that the accuracy of F2 is, statistically, significantly better than F1. In this study, we employ a one-sided DM test to assess the forecasting performance of the proposed models. We choose $d_t^{F1, F2} = |e_{1t}| - |e_{2t}|$ as the loss function.

6.3. Walk forward nested cross-validation

To avoid over-fitting, it is common to include a validation set to evaluate the generalisation ability of the training model. The cross-validation is referred to as a method for tuning the hyperparameters and producing robust measurements of model performance. In [57], a nested cross-validation procedure was introduced, which considerably reduced the bias and provided an almost unbiased estimate of the true error. Because new observations become available over time, in time series modelling, we implement a Walk Forward Nested Cross-Validation in which the forecast rolls forward in time. More specifically, we successively consider each day as the test set and assign all previous data to the training set (Outer loop). The training set is split into a training subset and a validation set. The validation set data comes chronologically after the training subset (Inner loop). Walk forward validation involves moving along the time series one-time step at a time. The process is shown in Figure 12.

6.4. Data division

We divide the whole database into two subsets: a training set and a test set. The training set includes a training subset and a validation subset, as shown in the dashed box in Figure 12. We initially apportion the data set into training, validation, and test sets, with an 80-10-10 split. The magnitude of the test and validation set is anchored during the walk-forward test.

6.5. Data processing

For neural network models training, the input data is usually normalised to the intervals $[0,1]$. This is not only done because the normalised data will require less time to train, but the prediction performance will also increase. In addition, we linearly interpolate the missing data and eliminate duplicates due to daylight saving.

6.6. Ten experiments

Training algorithms for DL models have usually required the initialisation of the weights of neural networks from which to begin the iterative training [58]. The random initial conditions for an LSTM network can result in different performance each time a given configuration is trained. Thus, we employ ten experiments for each model to reduce the impact of the variability on performance evaluation. Models are evaluated after taking the average of experiments.

6.7. NARMAX

The NARMAX (Nonlinear AutoRegressive Moving Average with eXogenous input) model is the benchmark (trained with the optimal structure) for our case study. The statistical model is widely used in energy price forecasting to handle multiple nonlinear inputs [32, 59]. The equation is represented as:

$$y(t) = F^\ell \left[y(t-1), \dots, y(t-N_y), u(t), \dots, u(t-N_u), \varepsilon(t-1), \dots, \varepsilon(t-N_\varepsilon) \right] + \varepsilon(t) \quad (19)$$

where $u(t)$ is the input and $y(t)$ is the output time-series, $\varepsilon(t)$ is the prediction error, N_u , N_y and N_ε are the input, output and prediction error lags, respectively, and F^ℓ is a nonlinear function.

6.8. SHAP

SHAP⁵ (SHapley Additive exPlanations) is a game theoretic method to explain the output of machine learning models [60, 61, 62]. The Shapley value is used to assess the feature relevance relative to the expectation of the output [63]. In this study, we use SHAP values to interpret the impact of certain values of a given feature on the expected price prediction. In particular, a Kernel SHAP is used for explaining an optimal SVR model obtained by grid-search on the dataset.

6.9. Parameters of feature selection methods

The applied configuration of PSO is $[c_1: 0.5, c_2: 0.3, w: 0.7]$ and the stop condition is satisfied after 10,000 iterations. For GA, the crossover possibility and mutation possibility are 0.5 and 0.2, respectively. The population size is 100 and the maximum number of generations is 10,000. On the basis of the predictive ELM, the amount of the selected features by PSO-ELM and GA-ELM is automatically set to 30. For the sake of input consistency, the magnitude of the selected features of the rest of the models is set to 30 as well. For the PC method, we rank all features attributable to the correlation coefficients and select the first 30 features. In terms of RFE-SVR, we rank features by importance, discard the least important features, and refit the model until 30 features remain. The regularisation parameter λ in Lasso regression is 0.02.

⁵The Python package SHAP is available at <https://github.com/slundberg/shap>

Table 2
The proposed models.

Mode	Model Explanation
M0	Benchmark: NARMAX model
M1	Filter-based method: PC-LSTM model
M2	Wrapper-based method: PSO-ELM-LSTM model
M3	Wrapper-based method: GA-ELM-LSTM model
M4	Wrapper-based method: RFE-SVR-LSTM model
M5	Embedded-based method: LASSO-LSTM model
M6	Autoencoder method: LSTM-LSTM Encoder-Decoder model
M7	Autoencoder method: CNN-LSTM Encoder-Decoder model
M8	Autoencoder method: CovLSTM Encoder-Decoder model
M9	Two-stage method: PC-LSTM-LSTM Encoder-Decoder model
M10	Two-stage method: PSO-ELM-LSTM-LSTM Encoder-Decoder model
M11	Two-stage method: GA-ELM-LSTM-LSTM Encoder-Decoder model
M12	Two-stage method: RFE-SVR-LSTM-LSTM Encoder-Decoder model
M13	Two-stage method: LASSO-LSTM-LSTM Encoder-Decoder model

6.10. Network Hyperparameters

Our study aims at investigating the applications and impacts of different types of feature selection methods in a predictive LSTM architecture. We use a coherent configuration of a specific LSTM model for comparison and do not perform an extensive hyperparameter optimisation to search for the optimal configuration. After an inexhaustive grid search, we constructed our prediction model from an LSTM model with a single hidden layer of 300 units, followed by a fully connected dense layer with 100 neurons that precedes the output layer. The LSTM encoder has a hidden layer with 300 units. In the CNN-LSTM Encoder-Decoder model, the CNN encoder has two convolutional layers, with 96 unites to amplify any salient features, followed by a max-pooling layer. In the ConvLSTM Encoder-Decoder model, the encoder is a convolutional layer with 64 units. The input sequence length is 14 days (2 weeks, commonly used in EPF). The optimiser is the Adam algorithm, and the loss function is Mean Squared Error (MSE).

7. Results

In this section, we report the empirical results obtained by the application of the introduced models. For similarity of presentation, the list of models and their acronyms is shown in Table 2.

7.1. Analysis of empirical results

The results of the feature selection are shown in Table 3. In Table 4, the DM test results indicate the proposed LSTM models are overwhelmingly better than the benchmark M0. Table 5 exhibits the prediction results of all the models and Figure 13 shows that of the LSTM models from ten experiments, measured in terms of SMAPE. As seen in Figure 13, of all the models, M4, M5, and M6 perform better than the others. The SMAPE results for M1, M2, M3, M4, M5, M6, M7 and M8 are shown in Table 6. The MAD, RMSE and MAPE are shown in Appendix Tables A.8, A.9, and A.10. From Table 3, we can see that M1 selects all the day-ahead prices. It is not surprising

that the day-ahead prices from different bidding areas are more relevant to the Nord Pool system price than other feature variables. However, the over-selection results in the information redundancies. Compared to M1, the wrapper-based methods eliminate several price variables rather than the other categories of variables. We can see that the two computationally intensive wrapper-based M2 and M3 do not perform better than the others. The optimisation methods have the problem of trapping in the same local optima. Although re-setting and experimenting can increase the chance of avoiding the traps, when dealing with high dimensional data sets, the optimisation methods still cannot guarantee they will find a global optimum solution and they are not suitable for all cases [64]. The straightforward concept and fast computation of ELM contributed to its widespread application in an exhaustive grid search, but it does not consider the sequential relationships in time series data, as with other traditional neural networks. This could be the reason why the two methods eliminate the lag-1 system price as an input. For the Lasso-regression method M5, we can summarise that it puts more emphasis on electricity transmission. Thus, the results show that nonlinear methods M4 and M5 are better on account of various feature selection in EPF. In addition, we find that M6 performs better than M7 and M8. Our results indicate that LSTM is a better feature filter than convolutional neural networks for time series problems.

Table 3 The results of features selection.

Feature	Feature selection model				
	M1	M2	M3	M4	M5
F1	✓	✗	✗	✓	✓
F2	✓	✓	✓	✓	✓
F3	✓	✗	✗	✓	✓
F4	✓	✓	✗	✓	✗
F5	✓	✗	✗	✗	✗
F6	✓	✗	✗	✗	✗
F7	✓	✗	✗	✗	✗
F8	✓	✓	✗	✗	✗
F9	✓	✗	✗	✓	✗
F10	✓	✗	✗	✓	✓
F11	✓	✓	✗	✓	✓
F12	✓	✗	✓	✓	✓
F13	✓	✓	✓	✓	✓
F14	✓	✗	✓	✗	✗
F15	✓	✗	✗	✗	✗
F16	✓	✗	✗	✗	✗
F17	✓	✗	✓	✗	✗
F18	✓	✓	✗	✓	✓
F19	✗	✓	✗	✓	✗
F20	✗	✓	✓	✓	✗
F21	✗	✗	✓	✗	✗

Continued on next column

Continued from previous column

Feature	Feature selection model				
	M1	M2	M3	M4	M5
F22	✗	✓	✓	✓	✗
F23	✗	✓	✗	✓	✗
F24	✓	✓	✓	✗	✗
F25	✗	✗	✗	✓	✓
F26	✗	✗	✓	✓	✓
F27	✓	✓	✓	✗	✓
F28	✗	✓	✓	✗	✗
F29	✗	✗	✗	✓	✓
F30	✗	✓	✗	✗	✓
F31	✗	✓	✗	✓	✗
F32	✗	✓	✓	✓	✓
F33	✓	✓	✗	✗	✗
F34	✓	✗	✓	✓	✓
F35	✗	✗	✗	✓	✓
F36	✗	✓	✓	✓	✓
F37	✗	✗	✗	✓	✗
F38	✓	✓	✓	✓	✗
F39	✓	✓	✓	✓	✓
F40	✗	✗	✓	✗	✗
F41	✓	✓	✗	✓	✓
F42	✗	✗	✗	✗	✗
F43	✓	✗	✓	✓	✗
F44	✓	✓	✓	✓	✓
F45	✓	✗	✓	✗	✗
F46	✗	✓	✗	✗	✓
F47	✗	✗	✗	✗	✗
F48	✗	✗	✗	✓	✓
F49	✗	✗	✓	✗	✓
F50	✗	✓	✓	✗	✓
F51	✗	✓	✗	✗	✓
F52	✗	✓	✓	✗	✗
F53	✗	✗	✗	✓	✓
F54	✗	✗	✓	✗	✓
F55	✗	✗	✗	✗	✗
F56	✗	✗	✓	✗	✗
F57	✗	✓	✓	✗	✗
F58	✗	✗	✓	✗	✓
F59	✓	✓	✓	✗	✓
F60	✓	✓	✓	✗	✗
F61	✗	✓	✗	✗	✓
F62	✗	✗	✗	✗	✗

Note: ✓ denotes that the feature is selected;

✗ denotes that the feature is not selected.

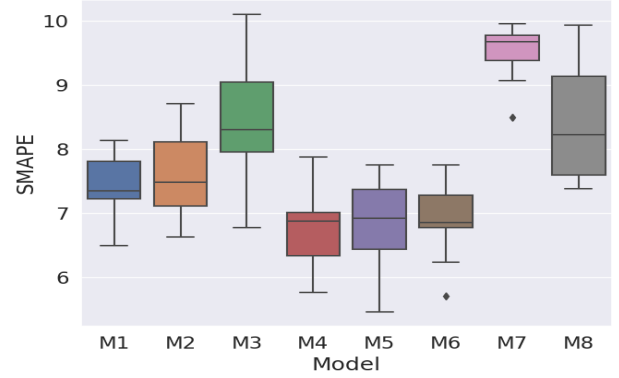


Figure 13 The SMAPEs of 10 experiments for M1, M2, M3, M4, M5, M6, M7 and M8.

We show the comparison of the SMAPE of the two-step and the two-stage models in Figure 14. From Figure 14, it can be seen that M3 and M4 have been improved by applying LSTM-LSTM as predictors. We use a one-sided DM test to detect whether the two-stage LSTM models are statistically better than two-step LSTM-LSTM models. The results are shown in Table 7. The superior features selection from M4 (RFE-SVR) provides the possibility for autoencoder models to further process it, to obtain more meaningful information.

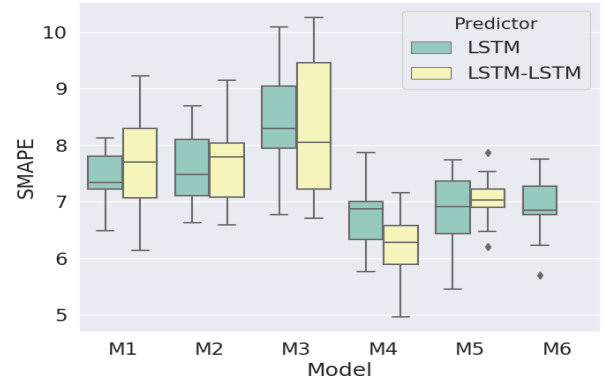


Figure 14 The comparison of SMAPEs between two-step LSTM models and two-stage LSTM-LSTM models.

Additionally, we detect the forecasting performance for 24 hourly system prices. Figures 15, 16 and 17 show the results for the three peak hours: H8 (07 - 08), H12 (11 - 12) and H18 (17 - 18), respectively, measured in terms of SMAPE. We observe that the feature selections influence the forecasting accuracy and the models M4 and M5 are still relatively stable, performing better than other models.

7.2. Analysis of feature impact

Figure 18 shows the features' ranking and impact on the predicted price in terms of the selected features of the RFE-SVR model (M4), which is the model with the best performance. From Figure 18a, we can observe that the features from the

Table 4

The results of the one-sided DM test.

F1 \ F2	M0	M1	M2	M3	M4	M5	M6	M7	M8
M0		5.83***	4.99***	3.90***	6.65***	7.09***	6.60***	4.61***	4.27***
M1	-5.83***		-1.15	-1.67*	2.31**	2.98***	1.59#	-0.16	0.88
M2	-4.99***	1.15		-0.91	2.70***	3.55***	3.84***	0.84	-0.20
M3	-3.90***	1.67*	0.91		3.19***	4.01***	4.31***	1.33	-0.97
M4	-6.65***	-2.31**	-2.70***	-3.19***		1.12	-0.23	-1.64#	2.57**
M5	-7.09***	-2.98***	-3.55***	-4.01***	-1.12		-0.97	-2.33**	3.19***
M6	-6.60***	-1.59#	-3.84***	-4.31***	0.23	0.97		-1.44	3.54***
M7	-4.61***	0.16	-0.84	-1.33	1.64#	2.33**	1.44		0.66
M8	-4.27***	-0.88	0.20	0.97	-2.57**	-3.19***	-3.54***	-0.66	

Note: ***, **, * and # denote 1%, 5%, 10%, and 15% significance levels, respectively. The positive sign of the DM value indicates that F2 is better F1. The negative sign of the DM value indicate that F1 is better F2.

Table 5

The SMAPE of M0, M1, M2, M3, M4, M5, M6, M7 and M8.

Model	M0	M1	M2	M3	M4	M5	M6	M7	M8
SMAPE	10.07	6.25	6.58	7.06	5.29	4.89	5.20	6.14	6.53

Table 6

The SMAPE (%) results for M1, M2, M3, M4, M5, M6, M7 and M8.

	M1	M2	M3	M4	M5	M6	M7	M8
count	10	10	10	10	10	10	10	10
mean	7.42	7.58	8.46	6.76	6.85	6.87	9.51	8.38
std	0.50	0.67	0.95	0.65	0.72	0.60	0.44	0.90
min	6.49	6.63	6.77	5.76	5.46	5.71	8.49	7.38
25%	7.22	7.10	7.95	6.33	6.43	6.77	9.38	7.59
50%	7.34	7.48	8.30	6.87	6.91	6.85	9.67	8.22
75%	7.81	8.10	9.05	7.01	7.37	7.27	9.77	9.13
max	8.13	8.70	10.09	7.87	7.74	7.75	9.95	9.93

Note: 25%, 50%, and 75% denote 25%, 50%, and 75% percentiles.

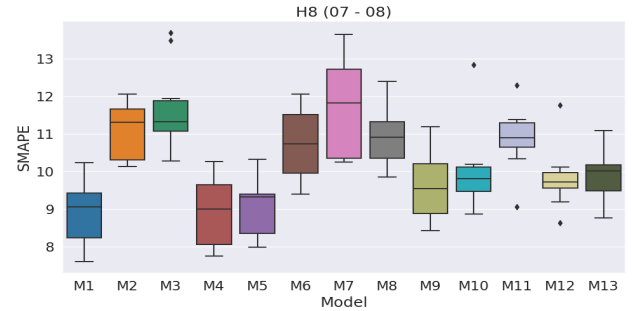
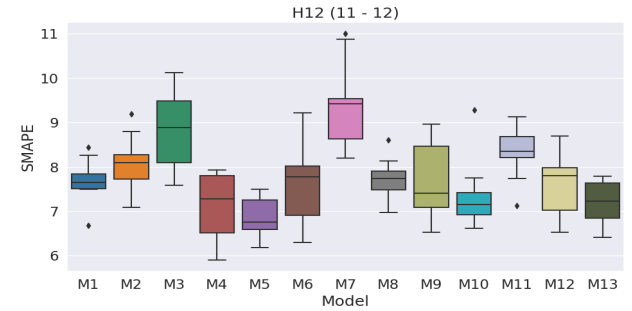
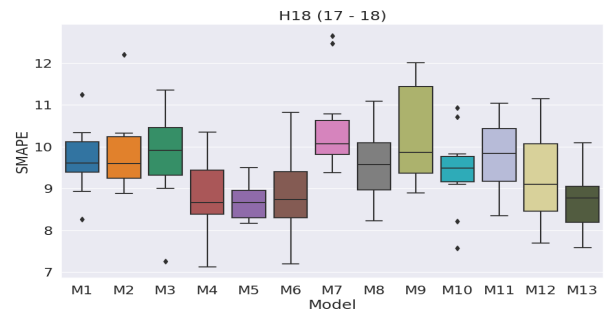
Table 7

The results of the one-sided DM test when comparing two-step models (F1) and two-stage models (F2).

F1	M1	M2	M3	M4	M5
	-0.6039	0.2222	2.4556 ***	2.4524 ***	-1.7053 ***
F2	M9	M10	M11	M12	M13

Note: ***, **, * and # denote 1%, 5%, 10%, and 15% significance levels, respectively. The positive sign: F2 is better F1. The negative sign: F1 is better F2.

Nordic market with the most significant impact are Nordic production prognosis (F25) and consumption prognosis (F37). The features from DE markets (F35, F23, F41 and F29) are more important than other cross-border markets. This can be explained by the fact that the German market has the most elec-

**Figure 15** The SMAPEs of 10 experiments for predicting H8.**Figure 16** The SMAPEs of 10 experiments for predicting H12.**Figure 17** The SMAPEs of 10 experiments for predicting H18.

tricity cables and the highest electricity exports to the Nordic market. This indicates that it is critical to consider features from

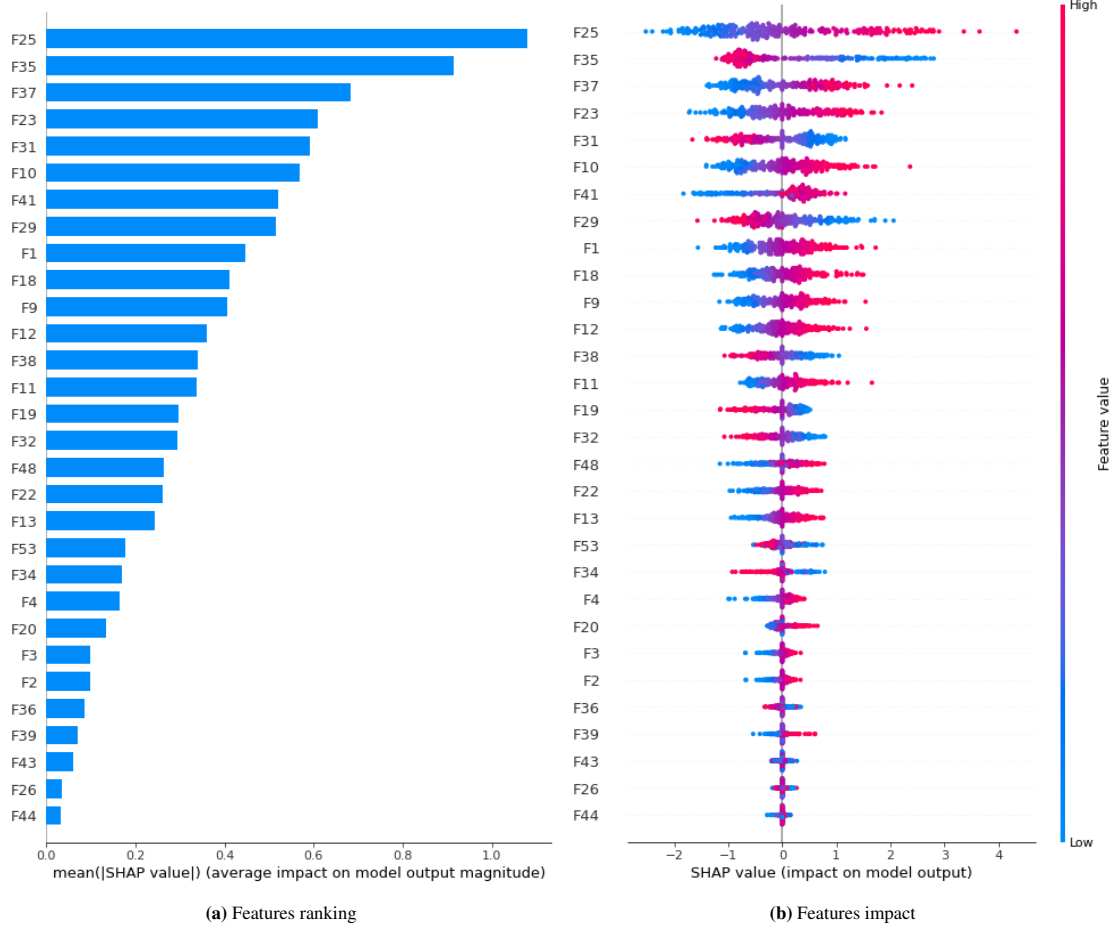


Figure 18 The feature ranking and feature impact of the selected features of RFE-SVR. (a) bar chart of the average SHAP value magnitude which shows the features' importance. (b) a set of beeswarm plots, where each dot corresponds to an individual day-ahead price. The dot's position on the x-axis shows the impact that feature has on the model's prediction for that price. Multiple dots landing at the same x position pile up to show density.

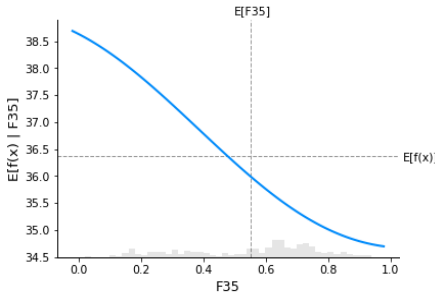
cross-border markets with increasing interconnections across Europe for EPF. From Figure 18b, we can see that a high value of Nordic production prognosis (F25) or consumption prognosis (F37) elevates the predicted price; and a low value of DE consumption (F35), with a long right tail, higher the predicted price. The trend of long-tail reaching to the right, but not to the left, indicates the extreme values of DE consumption can significantly raise the predicted price, but cannot significantly lower the price.

Figure 19a demonstrates the negative relationship between DE consumption and its conditional expectation of the predicted price. If the DE consumption has a high value, then it tends to revert to its expectation ($\mathbb{E}[F35]$). Thus, the downward expectation of DE consumption will lead to the expected decline of the import demand from the Nordic market, which further decreases the predicted price based on its expectation ($\mathbb{E}[f(x)]$). Figure 19b represents the change in predicted price as DE consumption changes. Vertical dispersion at a single value of DE consumption represents interaction effects with other features. For example, the interaction effect of DE consumption with Nordic production (F19) is shown in Figure 19c. The SHAP dependence plot highlights that the impact differs with different values of Nordic production. The results reveal

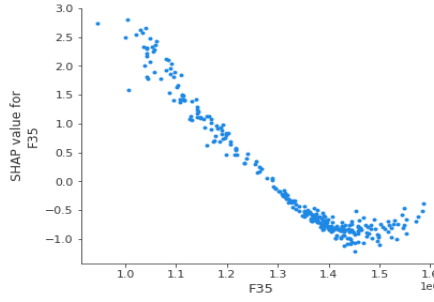
that the price prediction is less sensitive to DE consumption when the value of Nordic production is high. In such a case, the information from the Nordic market rather than cross-border countries drives the system-price prediction.

We can see that the majority of the EUR/NOK (F43) dots has no contribution to the changes in the predicted price (the value of y-axis is zero) in Figure 20. Besides, there is no obvious interaction effect between the Nordic production and EUR/NOK exchange rate on the predicted price. We see this because the red points are randomly distributed below and above a SHAP value of zero. However, we can observe that more red dots are on the right side than on the left side. This indicates that a depreciation of the NOK can stimulate the electricity export, and further prompt the Nordic production.

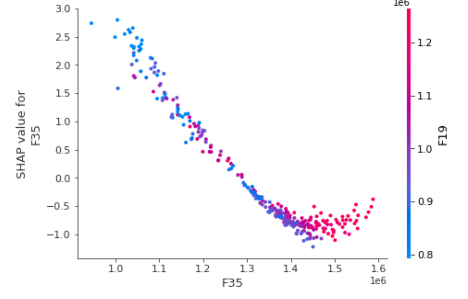
From Figure 21, we can find that the predicted price is expected to increase when we observe a high DK1 \rightarrow DE flow (indicating that the Nordic electricity price is relatively low). Meanwhile, a high flow from DE to DK1 means the price is high, and the price is expected to decline. In addition, an interaction effect of the DK1 $\leftarrow \rightarrow$ DE flow with the DE production prognosis shows that the flow has less impact on the predicted price with high expected production in Germany. Thus, the high production prognosis from cross-border countries will lead to a



(a) SHAP partial dependence plot of DE consumption



(b) SHAP dependence plot of DE consumption



(c) SHAP dependence plot of the interaction effect of DE consumption with Nordic production (F19)

Figure 19 The SHAP partial dependence (a) and dependence (b, c) plot of DE consumption (F35). The grey histogram in (a) shows the distribution of the feature in the test dataset. For (a), x-axis means the normalised DE consumption. The x-axes in (b) and (c) are real value of the consumption.

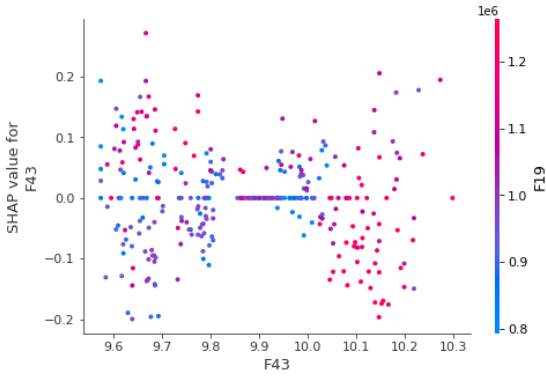


Figure 20 The SHAP dependence plot of EUR/NOK (F43). The interaction effect of EUR/NOK with Nordic production (F19).

high decline in the expected cross-border transmission. Its impact, consequently, will lead to a decrease in the price formation on the following day.

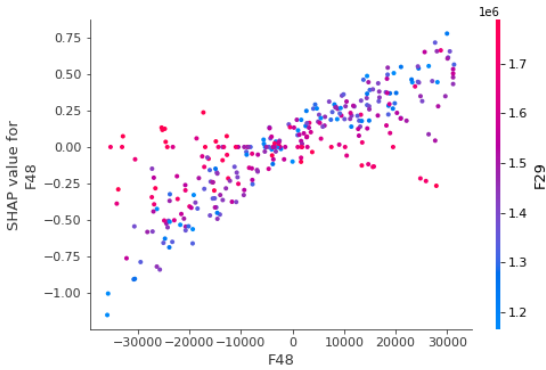


Figure 21 The SHAP dependence plot of DK1 <-> DE flow (F48). The interaction effect of DK1 <-> DE flow with DE production prognosis (F29).

Last but not least, not all of the cross-border electricity flows and flow deviations are helpful for forecasting. The reason for this is that, in many cases, the flow capacity is fully occupied. The lack of variability results in their inability to provide useful information for forecasting. An example of the flow and flow deviations between FI and Russia can be seen in Figure 22. However, this implies the potential for more electrical power transmission across the Europe-wide market in increasing the

overall socio-economic benefits.

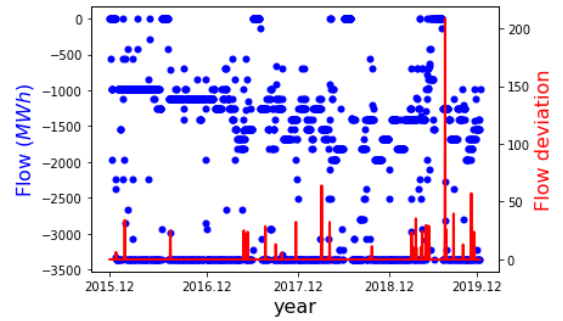


Figure 22 FI <-> Russia flow (F54) (blue dots) versus FI <-> Russia flow deviation (F62) (red line).

7.3. Discussion of practical importance

An accurate prediction can be highly beneficial for the electricity market participants in practice. A power market firm that is capable of forecasting the volatile electricity price with a reasonable level of accuracy can reduce trading risk and maximise profits in the day-ahead market, by adjusting its bidding strategy and the schedule for production or consumption. More specifically, a 1% improvement in MAPE of forecast accuracy (within a 5% to 14% range), leads to about 0.1% - 0.35% cost reduction [65]. On average, a 1% reduction in the MAPE of short-term price forecasts can result in savings of \$1.5 million per year, for a typical medium-sized utility company with 5-GW peak load [66, 29]. Furthermore, electricity is economically non-storable and the imbalance between production and consumption can result in power system instability [67]. Accurate electricity forecasting allows energy firms to efficiently organise production or consumption, and this improves the stability of the power system. In addition, the Nord Pool system price is an index reflecting the Nordic Day-ahead market for electricity and it is a commodity benchmark and a regulated data benchmark [68]. Accurate forecasts can be regarded as being a reference for the Nord Pool market and its integrated markets to perform operation and regulation.

8. Conclusion

In this paper, we present three LSTM-based DL architectures for the EPF. This study puts emphasis on the influence of feature selection methods in the proposed hybrid models. In particular, we compare the prediction performance of the two-step feature selection, the autoencoder, and two-stage feature selection models based on the empirical study on the Nord Pool day-ahead system price. In addition, we employ a SHAP method to evaluate the features' importance and impact on predicting this price. The main findings are: (1) We conclude that the different feature selection methods will lead to different feature selections. As input, diverse features will have a comparably significant impact on increasing the performance of LSTM-based predictive models. (2) The two-stage models can improve the forecasting accuracy of two-step models to some extent. The superior feature selection from the RFE-SVR model allows the autoencoder model to detect more meaningful information for more accurate prediction. (3) The features from the German market (with the most power cables linking to Nord Pool) are more significant for EPF than others. This indicates that more interconnections will increase the cross-border influence on EPF. (4) Compared to other features, the exchange rates are relatively less important. (5) Flow deviation cannot significantly contribute to the price prediction because of its lack of variability. In many cases, the expected flow capacity is fully occupied. This implies more interconnections are expected for an efficient Europe-wide electricity market.

For future studies, several extensions of the current study can be developed. Indeed, although the forecasting performance of the proposed models is considerable, we do not conduct an extensive grid search to optimise hyperparameters. It is reasonable to believe that the LSTM-based models with more comprehensive architecture will achieve a better forecasting performance. The results will benefit spot electricity traders and policymakers, who make decisions based on accurate price predictions. Moreover, we envision that more testing on other feature selection models can obtain more, different feature selection subsets. They can provide more possibilities for researchers and industries to understand how different features affect prediction accuracy. Finally, the study was carried out using the data from the Nord Pool market, but the generality of the proposed models ensures a possible application to other integrated markets, like EPEX and OMIE.

9. Acknowledgement

This work acknowledges research support by COST Action "Fintech and Artificial Intelligence in Finance - Towards a transparent financial industry" (FinAI) CA19130. This research has been performed within the +CityxChange⁶ (Positive City ExChange) project under the Smart Cities and Communities topic that has received funding from the European

Union's Horizon 2020 research and innovation programme under Grant Agreement No. 824260. Critical comments and advice from Florentina Paraschiv and Frode Kjærland are gratefully acknowledged.

Appendix A.

Table A.8

The MAD results for M1, M2, M3, M4, M5, M6, M7 and M8.

	M1	M2	M3	M4	M5	M6	M7	M8
count	10	10	10	10	10	10	10	10
mean	2.78	2.99	3.31	2.54	2.61	2.67	3.67	3.28
std	0.17	0.29	0.40	0.25	0.30	0.25	0.15	0.38
min	2.42	2.58	2.64	2.16	2.04	2.20	3.30	2.84
25%	2.72	2.77	3.10	2.34	2.45	2.59	3.65	2.99
50%	2.77	2.95	3.25	2.59	2.65	2.65	3.69	3.18
75%	2.92	3.24	3.56	2.63	2.74	2.85	3.73	3.60
max	2.98	3.41	3.93	2.99	3.00	3.09	3.89	3.95

Note: 25%, 50%, and 75% denote 25%, 50%, and 75% percentiles.

Table A.9

The RMSE results for M1, M2, M3, M4, M5, M6, M7 and M8.

	M1	M2	M3	M4	M5	M6	M7	M8
count	10	10	10	10	10	10	10	10
mean	3.60	3.79	4.22	3.25	3.46	3.33	4.74	3.99
std	0.24	0.42	0.55	0.33	0.43	0.32	0.29	0.46
min	3.17	3.15	3.35	2.61	2.79	2.85	4.13	3.50
25%	3.51	3.45	3.87	3.04	3.27	3.13	4.62	3.60
50%	3.64	3.78	4.16	3.30	3.50	3.30	4.90	3.92
75%	3.71	4.05	4.55	3.45	3.71	3.47	4.91	4.33
max	3.96	4.51	5.11	3.73	4.08	3.91	4.97	4.77

Note: 25%, 50%, and 75% denote 25%, 50%, and 75% percentiles.

Table A.10

The MAPE (%) results for M1, M2, M3, M4, M5, M6, M7 and M8.

	M1	M2	M3	M4	M5	M6	M7	M8
count	10	10	10	10	10	10	10	10
mean	7.24	7.83	8.75	6.66	6.79	7.01	9.31	8.73
std	0.46	0.73	1.05	0.65	0.78	0.68	0.47	1.06
min	6.28	6.82	6.89	5.72	5.32	5.67	8.56	7.50
25%	7.05	7.22	8.19	6.18	6.35	6.84	9.08	7.90
50%	7.24	7.71	8.62	6.73	6.85	6.95	9.16	8.44
75%	7.61	8.49	9.35	6.87	7.15	7.45	9.50	9.59
max	7.80	8.93	10.37	7.86	7.91	8.09	10.27	10.66

Note: 25%, 50%, and 75% denote 25%, 50%, and 75% percentiles.

⁶<https://cityxchange.eu/>

References

- [1] Weron R. Modeling and forecasting electricity loads and prices: A statistical approach. Wiley; 2006.
- [2] Bunn D. Modelling prices in competitive electricity markets. Wiley; 2004.
- [3] Nogales FJ, Contreras J, Conejo AJ, Espinola R. Forecasting next-day electricity prices by time series models. *IEEE Transactions on Power Systems* 2002;17(2):342–348. <https://doi.org/10.1109/TPWRS.2002.1007902>.
- [4] Bunn DW. Forecasting loads and prices in competitive power markets. *Proceedings of the IEEE* 2000;88(2):163–169. <https://doi.org/10.1109/5.823996>.
- [5] Weron R. Electricity price forecasting: A review of the state-of-the-art with a look into the future. *International Journal of Forecasting* 2014;30(4):1030 – 1081. <https://doi.org/10.1016/j.ijforecast.2014.08.008>.
- [6] Nowotarski J, Weron R. Recent advances in electricity price forecasting: A review of probabilistic forecasting. *Renewable and Sustainable Energy Reviews* 2018;81:1548 – 1568. <https://doi.org/10.1016/j.rser.2017.05.234>.
- [7] Ventosa M, Baillo A, Ramos A, Rivie M. Electricity market modeling trends. *Energy Policy* 2005;33(7):897 – 913. <https://doi.org/10.1016/j.enpol.2003.10.013>.
- [8] Kiose D, Voudouris V. The acwem framework: An integrated agent-based and statistical modelling laboratory for repeated power auctions. *Expert Systems with Applications* 2015;42(5):2731 – 2748. <https://doi.org/10.1016/j.eswa.2014.11.024>.
- [9] Burger M, Schindlmayr G, Graeber B. Managing Energy Risk: An Integrated View on Power and Other Energy Markets. Wiley; 2007.
- [10] Islyayev S, Date P. Electricity futures price models: Calibration and forecasting. *European Journal of Operational Research* 2015;247(1):144 – 154. <https://doi.org/10.1016/j.ejor.2015.05.063>.
- [11] Weron R, Misiorek A. Forecasting spot electricity prices: A comparison of parametric and semiparametric time series models. *International Journal of Forecasting* 2008;24(4):744 – 763. <https://doi.org/10.1016/j.ijforecast.2008.08.004>.
- [12] Conejo AJ, Contreras J, Espínola R, Plazas MA. Forecasting electricity prices for a day-ahead pool-based electric energy market. *International Journal of Forecasting* 2005;21(3):435 – 462. <https://doi.org/10.1016/j.ijforecast.2004.12.005>.
- [13] Misiorek A, and Trueck S, Weron R. Point and interval forecasting of spot electricity prices: Linear vs non-linear time series models. *Studies in Nonlinear Dynamics & Econometrics* 2006;10(3). <https://doi.org/10.2202/1558-3708.1362>.
- [14] Gonzalez JP, Roque AMSMS, Pérez EA. Forecasting functional time series with a new Hilbertian ARMAX model: Application to electricity price forecasting. *IEEE Transactions on Power Systems* 2018;33(1):545–556. <https://doi.org/10.1109/TPWRS.2017.2700287>.
- [15] Catalao J, Mariano S, Mendes V, Ferreira L. Short-term electricity prices forecasting in a competitive market: A neural network approach. *Electric Power Systems Research* 2007;77(10):1297 – 1304. <https://doi.org/10.1016/j.epsr.2006.09.022>.
- [16] Keles D, Scelle J, Paraschiv F, Fichtner W. Extended forecast methods for day-ahead electricity spot prices applying artificial neural networks. *Applied Energy* 2016;162:218 – 230. <https://doi.org/10.1016/j.apenergy.2015.09.087>.
- [17] Peter S, Raglend I. Sequential wavelet-ANN with embedded ANN-PSO hybrid electricity price forecasting model for indian energy exchange. *Neural Comput & Applic* 2017;28:2277–2292. <https://doi.org/10.1007/s00521-015-2141-3>.
- [18] Hinton G, Deng L, Yu D, Dahl GE, rahman Mohamed A, Jaitly N, et al. Deep neural networks for acoustic modeling in speech recognition: The shared views of four research groups. *IEEE Signal Processing Magazine* 2012;29:82 – 97. <https://doi.org/10.1109/MSP.2012.2205597>.
- [19] Bahdanau D, Cho K, Bengio Y. Neural machine translation by jointly learning to align and translate. *arXiv:1409.0473 [cs.CL]* 2014; Available from: <http://arxiv.org/abs/1409.0473>.
- [20] Li L, Yuan Z, Gao Y. Maximization of energy absorption for a wave energy converter using the deep machine learning. *Energy* 2018;165:340 – 349. <https://doi.org/10.1016/j.energy.2018.09.093>.
- [21] Bengio Y, Simard P, Frasconi P. Learning long-term dependencies with gradient descent is difficult. *IEEE Transactions on Neural Networks* 1994;5(2):157–166. <https://doi.org/10.1109/72.279181>.
- [22] Lago J, Ridder FD, Schutter BD. Forecasting spot electricity prices: Deep learning approaches and empirical comparison of traditional algorithms. *Applied Energy* 2018;221:386 – 405. <https://doi.org/10.1016/j.apenergy.2018.02.069>.
- [23] Chang Z, Zhang Y, Chen W. Electricity price prediction based on hybrid model of adam optimized LSTM neural network and wavelet transform. *Energy* 2019;187:115804. <https://doi.org/10.1016/j.energy.2019.07.134>.
- [24] Kuo PH, Huang CJ. An electricity price forecasting model by hybrid structured deep neural networks. *Sustainability* 2018;10(4). <https://doi.org/10.3390/su10041280>.
- [25] Hastie T, Tibshirani R, Friedman J. The elements of statistical learning: data mining, inference and prediction. 2 ed.; Springer; 2009.
- [26] Li J, Cheng K, Wang S, Morstatter F, Trevino RP, Tang J, et al. Feature selection: A data perspective. *ACM Computing Surveys* 2017;50(6). <https://doi.org/10.1145/3136625>.
- [27] Ziel F, Steinert R, Husmann S. Forecasting day ahead electricity spot prices: The impact of the exaa to other european electricity markets. *Energy Economics* 2015;51:430 – 444. <https://doi.org/10.1016/j.eneco.2015.08.005>.
- [28] Panapakidis IP, Dagoumas AS. Day-ahead electricity price forecasting via the application of artificial neural network based models. *Applied Energy* 2016;172:132 – 151. <https://doi.org/10.1016/j.apenergy.2016.03.089>.
- [29] Lago J, De Ridder F, Vrancx P, De Schutter B. Forecasting day-ahead electricity prices in europe: The importance of considering market integration. *Applied Energy* 2018;211:890 – 903. <https://doi.org/10.1016/j.apenergy.2017.11.098>.
- [30] Uribe JM, Mosquera-López S, Guillen M. Characterizing electricity market integration in nord pool. *Energy* 2020;208:118368. <https://doi.org/10.1016/j.energy.2020.118368>.
- [31] Marcjasz G, Lago J, Weron R. Neural networks in day-ahead electricity price forecasting: Single vs. multiple outputs. *arXiv:2008.08006 [stat.AP]* 2020; Available from: <https://arxiv.org/abs/2008.08006>.
- [32] Johannessen NJ, Kolhe M, Goodwin M. Deregulated electric energy price forecasting in nordpool market using regression techniques. In: 2019 IEEE Sustainable Power and Energy Conference (ISPEC). 2019, p. 1932–1938. <https://ieeexplore.ieee.org/abstract/document/8975173>.
- [33] Greenfish. Shaping our electrical future: Moving towards an integrated european network. <https://www.greenfish.eu/shaping-our-electrical-future-moving-towards-an-integrated-european-network/>; 2019. [accessed 13 September 2020].
- [34] Hochreiter S, Schmidhuber J. Long short-term memory. *Neural Computation* 1997;7(4):1735 – 1780. <https://doi.org/10.1162/neco.1997.9.8.1735>.
- [35] Gers FA, Schmidhuber J. Recurrent nets that time and count. In: Proceedings of the IEEE-INNS-ENNS International Joint Conference on Neural Networks. IJCNN 2000. Neural Computing: New Challenges and Perspectives for the New Millennium; vol. 3. 2000, p. 189–194. <https://doi.org/10.1109/IJCNN.2000.861302>.
- [36] Graves A, Schmidhuber J. Framewise phoneme classification with bidirectional LSTM and other neural network architectures. *Neural Networks* 2005;18(5):602 – 610. <https://doi.org/10.1016/j.neunet.2005.06.042>; *IJCNN* 2005.
- [37] Cho K, van Merriënboer B, Gulcehre C, Bahdanau D, Bougares F, Schwenk H, et al. Learning phrase representations using RNN encoder-decoder for statistical machine translation. *arXiv:1406.1078 [cs.CL]* 2014; Available from: <https://arxiv.org/abs/1406.1078>.
- [38] Graves A. Generating sequences with recurrent neural networks. *arXiv:1308.0850 [cs.NE]* 2013; Available from: <https://arxiv.org/abs/1308.0850>.
- [39] Chandrashekar G, Sahin F. A survey on feature selection methods. *Computers & Electrical Engineering* 2014;40(1):16 – 28. <https://doi.org/10.1016/j.compeleceng.2013.11.024>; 40th-year commemorative issue.
- [40] Chen X, Zeng X, van Alphen D. Multi-class feature selection for tex-

- ture classification. *Pattern Recognition Letters* 2006;27(14):1685 – 1691. <https://doi.org/10.1016/j.patrec.2006.03.013>.
- [41] Nguyen HB, Xue B, Liu I, Andreae P, Zhang M. New mechanism for archive maintenance in PSO-based multi-objective feature selection. *Soft Computing* 2016;20:3927 – 3946. <https://doi.org/10.1007/s00500-016-2128-8>.
- [42] Shang L, Zhou Z, Liu X. Particle swarm optimization-based feature selection in sentiment classification. *Soft Computing* 2016;20:3821 – 3834. <https://doi.org/10.1007/s00500-016-2128-8>.
- [43] Zhou Y, Zhou N, Gong L, Jiang M. Prediction of photovoltaic power output based on similar day analysis, genetic algorithm and extreme learning machine. *Energy* 2020;204:117894. <https://doi.org/10.1016/j.energy.2020.117894>.
- [44] S. Krishnan G, S. S. A novel GA-ELM model for patient-specific mortality prediction over large-scale lab event data. *Applied Soft Computing Journal* 2019;80:525–533. 10.1016/j.asoc.2019.04.019.
- [45] Luo P, Zhu S, Han L, Chen Q. Short-term photovoltaic generation forecasting based on similar day selection and extreme learning machine. vol. 2018-January. 2018, p. 1–5. 10.1109/PESGM.2017.8273776.
- [46] Huang GB, Zhu QY, Siew CK. Extreme learning machine: Theory and applications. *Neurocomputing* 2006;70(1):489 – 501. <https://doi.org/10.1016/j.neucom.2005.12.126>.
- [47] Saraswathi S, Sundaram S, Sundararajan N, Zimmermann M, Nilsen-Hamilton M. ICGA-PSO-ELM approach for accurate multiclass cancer classification resulting in reduced gene sets in which genes encoding secreted proteins are highly represented. *IEEE/ACM Transactions on Computational Biology and Bioinformatics* 2011;8(2):452–463. <https://doi.org/10.1109/TCBB.2010.13>.
- [48] Chyzyk D, Savio A, Graña M. Evolutionary ELM wrapper feature selection for Alzheimer’s disease CAD on anatomical brain MRI. *Neurocomputing* 2014;128:73 – 80. <https://doi.org/10.1016/j.neucom.2013.01.065>.
- [49] Ahila R, Sadasivam V, Manimala K. An integrated PSO for parameter determination and feature selection of ELM and its application in classification of power system disturbances. *Applied Soft Computing* 2015;32:23 – 37. <https://doi.org/10.1016/j.asoc.2015.03.036>.
- [50] Whitley D. A genetic algorithm tutorial. *Statistics and Computing* 1994;4(2):65–85. 10.1007/BF00175354.
- [51] Herczeg S, Željka Ujević Andrijić, Bolf N. Development of soft sensors for isomerization process based on support vector machine regression and dynamic polynomial models. *Chemical Engineering Research and Design* 2019;149:95 – 103. <https://doi.org/10.1016/j.cherd.2019.06.034>.
- [52] Szegedy C, Wei Liu, Yangqing Jia, Sermanet P, Reed S, Anguelov D, et al. Going deeper with convolutions. In: 2015 IEEE Conference on Computer Vision and Pattern Recognition (CVPR). 2015, p. 1–9. <https://doi.org/10.1109/CVPR.2015.7298594>.
- [53] Sutskever I, Vinyals O, Le QV. Sequence to sequence learning with neural networks. In: Ghahramani Z, Welling M, Cortes C, Lawrence ND, Weinberger KQ, editors. *Advances in Neural Information Processing Systems* 27. Curran Associates, Inc.; 2014, p. 3104–3112. <https://arxiv.org/abs/1409.3215>.
- [54] Shi X, Chen Z, Wang H, Yeung DY, Wong Wk, WOO Wc. Convolutional LSTM network: A machine learning approach for precipitation nowcasting. In: Cortes C, Lawrence ND, Lee DD, Sugiyama M, Garnett R, editors. *Advances in Neural Information Processing Systems* 28. Curran Associates, Inc.; 2015, p. 802–810. <https://arxiv.org/pdf/1506.04214.pdf>.
- [55] Diebold FX, Mariano RS. Comparing predictive accuracy. *Journal of Business & Economic Statistics* 2002;20(1):134–144. <https://doi.org/10.1198/073500102753410444>.
- [56] Harvey D, Leybourne S, Newbold P. Testing the equality of prediction mean squared errors. *International Journal of Forecasting* 1997;13(2):281 – 291. [https://doi.org/10.1016/S0169-2070\(96\)00719-4](https://doi.org/10.1016/S0169-2070(96)00719-4).
- [57] Varma S, Simon R. Bias in error estimation when using cross-validation for model selection. *BMC Bioinformatics* 2006;7:91. <https://doi.org/10.1186/1471-2105-7-91>.
- [58] Goodfellow I, Bengio Y, Courville A. *Deep Learning*. The MIT Press; 2016.
- [59] McHugh C, Coleman S, Kerr D, McGlynn D. Daily energy price forecasting using a polynomial narmax model. In: Lotfi A, Bouchachia H, Gegov A, Langensiepen C, McGinnity M, editors. *Advances in Computational Intelligence Systems*. Cham: Springer International Publishing. ISBN 978-3-319-97982-3; 2019, p. 71–82.
- [60] Lundberg SM, Erion G, Chen H, DeGrave A, Prutkin JM, Nair B, et al. From local explanations to global understanding with explainable ai for trees. *Nature Machine Intelligence* 2020;2(1):56–67. 10.1038/s42256-019-0138-9.
- [61] Janzing D, Minorics L, Blöbaum P. Feature relevance quantification in explainable ai: A causal problem. 2019. [arXiv:1910.13413](https://arxiv.org/abs/1910.13413); available from: <https://arxiv.org/abs/1910.13413>.
- [62] Sundararajan M, Najmi A. The many shapley values for model explanation. 2020. [arXiv:1908.08474](https://arxiv.org/abs/1908.08474); available from: <https://arxiv.org/abs/1908.08474>.
- [63] Lundberg S, Lee SI. A unified approach to interpreting model predictions. 2017. [arXiv:1705.07874](https://arxiv.org/abs/1705.07874); available from: <https://arxiv.org/abs/1705.07874>.
- [64] Jamian JJ, Abdullah MN, Mokhlis H, Mustafa MW, Bakar AHA. Global particle swarm optimization for high dimension numerical functions analysis. *Journal of Applied Mathematics* 2014;<https://doi.org/10.1155/2014/329193>.
- [65] Zareipour H, Canizares CA, Bhattacharya K. Economic impact of electricity market price forecasting errors: A demand-side analysis. *IEEE Transactions on Power Systems* 2010;25(1):254–262. <https://doi.org/10.1109/TPWRS.2009.2030380>.
- [66] Uniejewski B, Nowotarski J, Weron R. Automated variable selection and shrinkage for day-ahead electricity price forecasting. *Energies* 2016;9(8). <https://doi.org/10.3390/en9080621>.
- [67] Kaminski V. *Energy markets. Risk Book*; 2013.
- [68] Nord Pool. *Nordic System Price*. <https://www.nordpoolgroup.com/4a7544/globalassets/download-center/day-ahead/methodology-for-calculating-nordic-system-price.pdf>; 2020. [accessed 13 September 2020].